ELSEVIER

Journal of Alloys and Compounds 446–447 (2007) 290–295

Journal of ALLOYS AND COMPOUNDS

www.elsevier.com/locate/jallcom

NMR studies of the aluminum hydride phases and their stabilities

Son-Jong Hwang [a,*], R.C. Bowman Jr. [b], Jason Graetz [c], J.J. Reilly [c], W. Langley [d], C.M. Jensen [d]

[a] *The Division of Chemistry and Chemical Engineering, California Institute of Technology, Pasadena, CA 91125, USA*
[b] *Jet Propulsion Laboratory, California Institute of Technology, Pasadena, CA 91109, USA*
[c] *Brookhaven National Laboratory, Department of Energy Sciences and Technology, Upton, NY 11973, USA*
[d] *Department of Chemistry, University of Hawaii, Honolulu, HI 96822, USA*

Received 27 October 2006; received in revised form 11 January 2007; accepted 11 January 2007
Available online 28 January 2007

Abstract

Multinuclear and multidimensional solid state NMR techniques including magic-angle-spinning (MAS) and multiple-quantum (MQ) MAS experiments have been used to characterize various AlH_3 samples. At least three distinct polymorphic AlH_3 phases have been prepared by desolvating the alane etherate product from its organometallic synthesis. MAS-NMR spectra for the ^1H and ^{27}Al nuclei have been obtained on a variety of AlH_3 samples that include the β- and γ-phases as well as the α-phase. ^{27}Al MAS NMR was found to respond with high sensitivity for showing differences in spatial arrangements of AlH_6 octahedra in the three polymorphs studied. Based on the characteristic NMR signatures determined, phase transition of the γ-AlH_3 to the α-AlH_3 was studied at room and high temperatures. Direct decomposition of the γ-AlH_3 to aluminum metal at room temperature was also unambiguously confirmed by NMR studies.

Keywords: Hydrogen storage materials; Gas–solid reactions; Nuclear resonances

1. Introduction

Aluminum hydride (AlH_3, alane) is a metastable solid with large hydrogen gravimetric (∼10 wt%) and volumetric (0.148 kg H_2/L) capacities. Because of its high potential as a hydrogen fuel carrier for automotive applications, there have recently been considerable interests in understanding and development of the material. Recently, various alane phases (e.g., α, β, and γ) were freshly prepared, characterized [1–4], and thermodynamics were determined [2,5]. Enhanced kinetics in thermal decomposition of AlH_3 was observed by Sandrock et al. [6,7] when dopants (e.g., LiH, Ti) were incorporated or particle sizes were varied. More importantly a number of structural studies of alane phases have appeared. There was a report on NMR characterization of three different AlH_3 phases by Hwang et al. [8] identifying distinctive Al sites depending on polymorphs, and very recently crystal structures of α′, β, and γ phases in deuteride forms (AlD_3) were reported by Brinks et al. [9–11] and by Yartys et al. [12]. Since the original organometallic synthesis of α and 6 other polymorphs by Brower et al. [13], the α-AlH_3 phase was, until recently, the only phase with a known complete crystal structure [14], implicating the remarkable advances being made in short period of time.

In this work, we present a brief overview of high resolution NMR studies on the structures and thermal stabilities of AlH_3 polymorphs (α, β, and γ phases). In the literature, solid state NMR studies of pure AlH_3 material were reported by Zogal et al. [15,16] who used α-AlH_3 material originally produced at Dow Chemical to measure ^{27}Al quadrupolar coupling constant and observe molecular hydrogen (H_2) that they attributed to being adsorbed on the hydride particle surfaces from a sharp line of ^1H static NMR seen at temperature as low as 10 K. Tarasov et al. [4] more recently used ^{27}Al static NMR to explore formation of Al metal [Al(M)] during thermal decomposition of AlH_3 and AlD_3 reporting the kinetics for temperatures between 360 K and 400 K, and giving an activation energy. Although there is a lack of high resolution studies of pure AlH_3 except our recent work [8], use of high resolution NMR methods has been successful in addressing structures and chemical transformation of complex metal hydride systems [17–19].

* Corresponding author. Tel.: +1 626 395 2323; fax: +1 626 568 8743.
E-mail address: sonjong@cheme.caltech.edu (S.-J. Hwang).

0925-8388/$ – see front matter © 2007 Elsevier B.V. All rights reserved.
doi:10.1016/j.jallcom.2007.01.115

Table 1
AlH_3 samples used for the NMR experiments

Sample description	ID code
α-AlH_3	BNL-H2963
α-AlH_3	Dow
α-AlH_3	UTRC
γ-AlH_3	BNL-H2990, BNL-H3013
γ-AlD_3	UH-3
α, β, γ-mixed	BNL-H2961

The magic angle spinning (MAS) NMR of AlH_3 for ^{27}Al nucleus ($I = 5/2$) with high power ^1H decoupling in general yields well resolved ^{27}Al signal of which isotropic chemical shift (δ_{iso}) and quadrupolar coupling parameters (C_Q, η, where C_Q is the quadrupolar coupling constant and η is the asymmetry parameter) become distinctive signatures for different polymorphs of AlH_3 [8]. The fact that Al is positioned in the center of a symmetric AlH_6 octahedron (for all three α, β, γ polymorphs) [9,10,13,14] results in weak contribution of quadrupolar coupling and consequently less broadened favorable NMR lineshapes. When more broadening is introduced due to higher quadrupolar effect, which is the case for the γ-AlH_3, two-dimensional (2D) multiple quantum (MQ) MAS technique [20,21] can be used to obtain spectra with improved resolution. Overall, NMR is sensitive enough to distinguish subtle differences originated from variations in arrangement of AlH_6octahedra in space: i.e., corner shared (α, β) versus edge shared (γ). In addition, NMR was proven to provide separate signals for corner shared octahedra packed in different space groups (α versus β and one of the γ sites) [8]. Once these ^{27}Al spectral fingerprints are determined, NMR becomes a straightforward tool in exploring phase changes during hydrogen desorption processes of AlH_3 both at room and high temperatures. It is the aim of the current work to demonstrate how effectively NMR can be employed to study structure changes and kinetics during the thermal decomposition of both the old Dow and freshly made AlH_3 samples with differing phase compositions.

2. Experimental description

The alane (i.e., AlH_3) materials are from four sources: (1) originally manufactured by the Dow Chemical Company in the 1970s, (2) recently prepared at Brookhaven National Laboratory (BNL), (3) freshly prepared at University of Hawaii (UH), and passivated α-AlH_3 from an unspecified Russian source provided by United Technologies Research Center (UTRC) as listed in Table 1. The general synthesis methods and procedures described by Brower et al. [13] were followed to make all alane materials as reported previously [1,2]. Powder X-ray diffraction was used to identify the initial phase compositions of the samples characterized by NMR. The Dow material was primarily the α-phase alane with 8.3 wt% hydrogen content that was virtually unchanged after ~30 years storage in air at ambient conditions. All initial NMR sample handling was performed in a glove box under an argon atmosphere. Later samples were exposed to air on purpose and examined for the build-up of oxide layers [22].

Solid state MAS NMR spectra were recorded using a Bruker Avance 500 MHz spectrometer with a wide bore 11.7 T magnet and employing a Bruker 4 mm CPMAS probe with extended variable temperature capability up to 300 °C. The spectral frequencies were 500.23 MHz for ^1H nucleus and 130.35 MHz for ^{27}Al nucleus. NMR shifts were reported in parts per million (ppm) when externally referenced to tetramethylsilane (TMS) and 1.0 M of $Al(NO_3)_3$ aqueous solution at 0 ppm for ^1H and ^{27}Al nuclei, respectively. The AlH_3 powder samples were packed into a 4 mm ZrO_2 rotor after minimal additional grinding and were sealed with a tight fitting kel-F cap [8]. Sample spinning was performed using dry nitrogen gas. A typical ^{27}Al MAS NMR spectrum was obtained at a sample spinning rate of 14.5 kHz and after a 0.3 μs single pulse (<π/18) with application of strong ^1H decoupling pulse of the two-pulse phase modulation (TPPM) scheme [23]. *In situ* variable temperature (VT) MAS NMR experiments on AlH_3 were performed at 8 kHz spinning rate using a ZrO_2 cap that allowed leaking of hydrogen gas desorbed at high temperatures. The MQ MAS experiment was performed using the z-filter method [24] at a spinning speed of 14 kHz and a two-dimensional (2D) spectrum was presented after a shearing transformation [21].

3. Results and discussion

3.1. ^{27}Al NMR of AlH_3 phases

The characteristic ^{27}Al NMR features are shown in Fig. 1 for three different AlH_3 phases. Pure α-AlH_3 phases show relatively well resolved static powder pattern arising from both satellite ($m = \pm 3/2 \leftrightarrow m \pm 1/2$ and $m = \pm 5/2 \leftrightarrow m = \pm 3/2$) and central transitions ($m = -1/2 \leftrightarrow m = +1/2$) of ^{27}Al ($I = 5/2$) nuclei at around ~0 ppm, representing six-coordinated Al in AlH_6 octahedron units which are all connected by corner-sharing in the 3D chain [14]. Its MAS spectrum under 14.5 kHz spinning significantly improves the resolution to yield a single line ~850 Hz wide at 5.5 ppm, which is ~5 times sharper than he static linewidth (4.5 kHz). In addition to the centerband, several spinning sidebands are also present with their intensity distribution expressing the shape of the static powder pattern. Analysis of both spectra using the QUASAR software [25] allowed us to extract NMR parameters (see Table 2). As expected, Al sitting in a symmetric octahedron experiences very little electric field gradient (efg) as indicated by a small C_Q value (~250 kHz). Three

Table 2
The quadrupole coupling parameters for ^{27}Al spectra in AlH_3 phases

Sample	Code	δ_{iso} (ppm)	C_Q (MHz)[a]	η	Relative conc.
α-AlH_3	BNL-H2963	5.8	0.25	0.1	1.0
γ-AlH_3	BNL-H2990	γ-I: 10.9	2.9	0.58	1.0[b]
		γ-II: 36.0	4.0	0.02	0.48[b]
α + β + γ-AlH_3	BNL-H2961	21.5[c]	0.38[c]	0.49[c] (0.14)	α:β:γ-I:γ-II = 0.22:0.36:0.31:0.11

[a] The contribution of chemical shift anisotropy ($\Delta\delta_{CSA}$) was not taken into account in the current work. The estimated quadrupolar parameters need further refinements to provide more accurate values, which is currently in progress. For reference, a rough estimation [17] indicated that ^{27}Al NMR could show $\Delta\delta_{CSA}$ as large as 25 (±10) ppm for Li_3AlH_6 octahedron.
[b] The intensity ratio was reported accidentally the opposite way in our previous report [8].
[c] The parameters are for the β-AlH_3 phase.

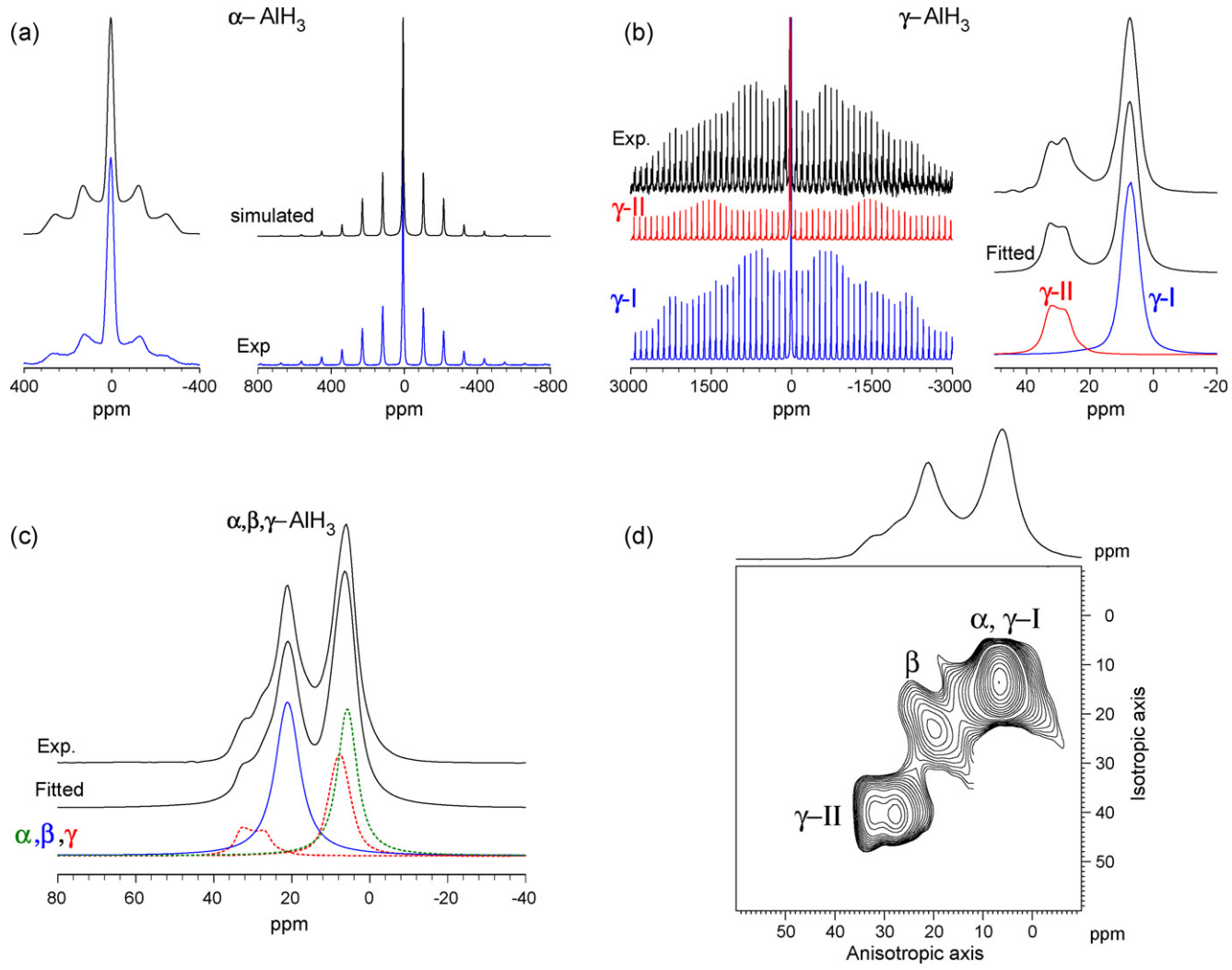

Fig. 1. ^{27}Al NMR spectra and simulations: (a) static and under MAS at 14.5 kHz of α-AlH_3, (b) γ-AlH_3 under MAS at 14 kHz for a wide manifold of spinning sidebands and the centerband, (c) characterization of β-AlH_3, and (d) A 2D MQMAS spectrum of mixed phase (BNL-H2961).

different α-AlH_3 materials (see Table 1: Dow, BNL, UTRC) were examined with NMR in the present work. Although the centerband of ^{27}Al MAS signal are nearly discernable among three samples, the ^{27}Al static NMR powder patterns (not shown) and the corresponding spinning sideband pattern in MAS spectra showed noticeable differences that are associated with variations in crystallinity, the amount of surface oxide layers (Al_2O_3), and crystal sizes of materials.

The NMR characterization of γ-AlH_3 phase was performed using the same approach on a BNL material with relatively high purity for the γ phase. Later, NMR analysis indicated that the γ-AlH_3 material also contained ~9 wt% of the α-AlH_3 phase and ~4 wt% of $LiAlH_4$ with negligible amount of Al(M). Unlike the α phase, Fig. 1(b) shows two sets of wide manifold of spinning sidebands distributed over 6000 ppm. This is a typical NMR signature of quadrupole nucleus under moderate quadrupolar coupling and with high crystallinity. Spectral fitting using the QUASAR (see simulated manifold of spinning sidebands for γ-I and γ-II) disclosed the presence of two different sites (see the centerband in Fig. 1(b)) with intensity ratio γ-I:γ-II = 2:1 and with the significantly larger quadrupolar coupling constants (see Table 2) compared to that of AlH_6 octahedra in the α-phase. The presence of two crystallographically different AlH_6 sites with 2:1 ratio was also revealed by recent crystal structure determinations of the γ-AlH_3 (or γ-AlD_3) by Brinks et al. [10] and Yartys et al. [12]. The fact that two AlH_6 octahedral sites are distorted in bond angles (Al–H–Al) and distances due to the nature of spatial arrangement of corner-sharing ($Al(I)H_6$) and edge-sharing ($Al(II)H_6$) octahedra in the γ phase is completely consistent with higher values in the quadrupolar interactions of NMR spectra. These associations between our NMR parameters with the crystal structures have allowed us to assign the two sites based on the site occupancy, and the assignment is listed in Table 2. The corner-sharing $Al(I)H_6$ octahedra, γ-II site, show well-defined powder pattern of the central transition ($m = +1/2 \leftrightarrow m = -1/2$) in the centerband (see Fig. 1(b)) due to the so called second order quadrupolar broadening. It is surprising since all corner-shared AlH_6 octahedra in the α and β phases show narrow and symmetric lineshapes. This is better understood now thanks to crystal structure studies showing that the corner-sharing $Al(I)H_6$

octahedra in the γ phase is highly distorted because of bonding to edge-sharing Al(II)H_6 in two different ways both in the plane and axial positions of octahedra and containing a large Al–H–Al bond angle [10,12].

For the β-AlH_3 phase, ^{27}Al NMR determination was performed using a material (i.e., BNL-H2961) crystallized with mixture of three different phases, which were identified by their X-ray diffraction peaks. Fitting of the experimental ^{27}Al MAS spectrum employing previously determined NMR parameters for both α and γ phases allowed us to separate out a spectral component that is quite similar to that of the α phase with an exception of a downfield shift in the isotropic chemical shift (see the deconvolution in Fig. 1(c) and Table 2). According to Brinks et al. [9], the β-AlH_3 phase consists of all corner-shared AlH_6 octahedra with a single crystallographic Al site and with similar structural parameters to those of the α-phase, consistent with our NMR result. The change in the isotropic shift can be attributed to the difference in the connectivity of octahedra. The mixture phase (α + β + γ) showed in addition a relatively strong initial Al(M) peak (not shown) even for freshly prepared samples compared to the others, implying that degradation occurs at room temperature much more rapidly. Fig. 1(d) shows a 2D MQMAS spectrum of the mixture phase with improved resolution, supporting our deconvolution of the one-dimensional (1D) spectrum. Note that the powder pattern seen for 1D MAS spectrum of the highly distorted γ-II site appears to be free from the second order broadening in the isotropic axis of 2D MQ MAS spectrum.

4. Decomposition studies of AlH_3 using NMR

^{27}Al NMR characterization in the previous section as well as ^{1}H and ^{2}H MAS NMR of AlH_3/AlD_3 phases plays a valuable role in studying chemical transformation of various AlH_3 phases: $AlH_3 \leftrightarrow Al(M) + 3/2H_2$. Note that unlike the ^{27}Al NMR, ^{1}H or ^{2}H MAS NMR in the solid AlH_3/AlD_3 phase did not provide distinctive signatures from different crystallographic sites. However, growth of sharp peaks at 4.4 ppm in ^{1}H or ^{2}H NMR can provide an easy check of desorption of hydrogen or deuterium molecules from the solid phase [8]. The resulting signature in ^{27}Al NMR is a decrease of intensity for peaks from AlH_3 phases with simultaneous growth of the Al(M) peak at 1640 ppm. The measure of peak intensities in the ^{27}Al MAS NMR spectra in turn gives rise to a handy *in situ* kinetics study. Here in the

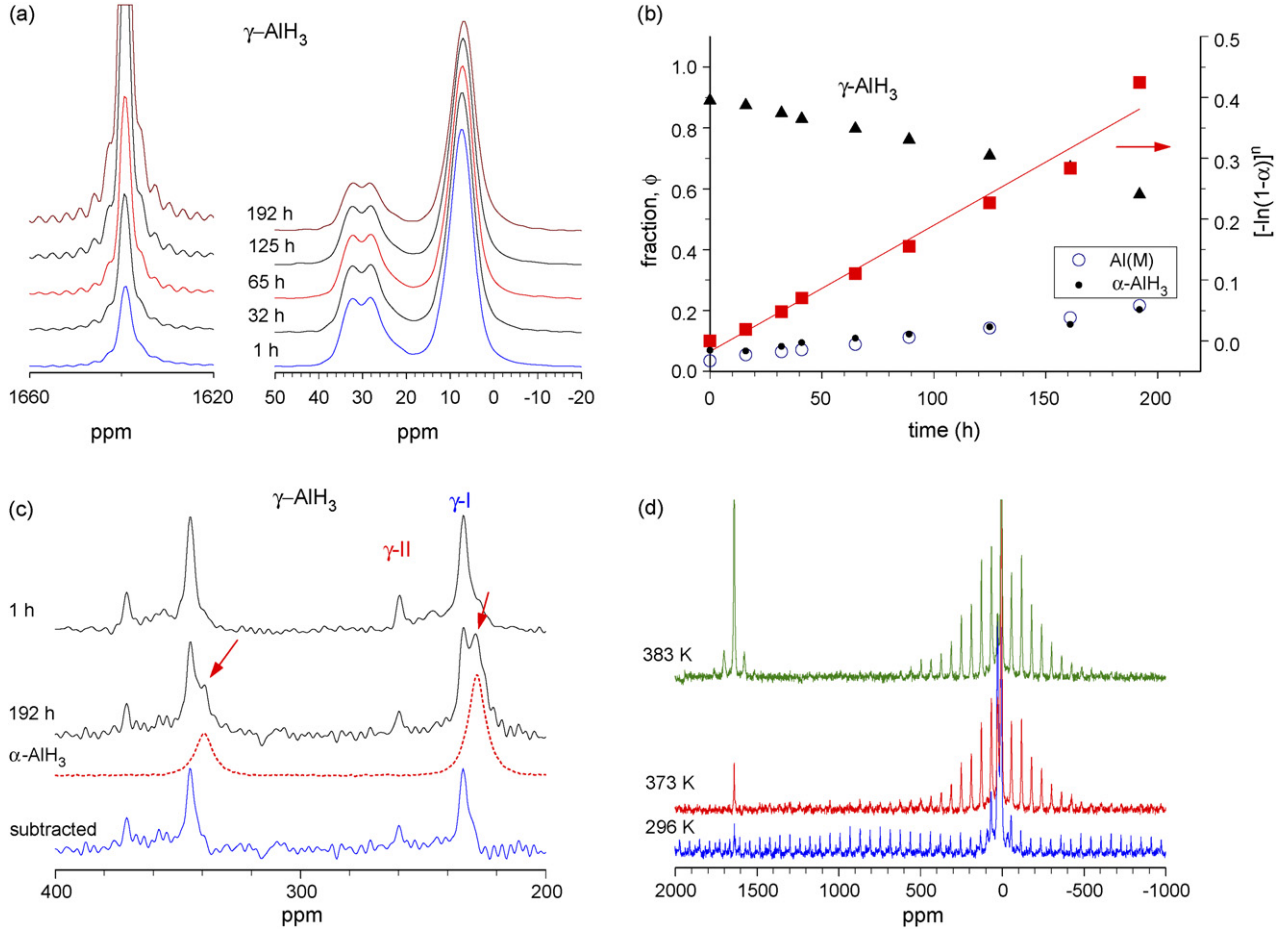

Fig. 2. (a) ^{27}Al MAS NMR spectra of γ-AlH_3 phase undergoing self-decomposition at room temperature. (b) Plot of fraction (ϕ) of γ-AlH_3, Al(M), and α-AlH_3 during the decomposition of the γ-AlH_3 sample, and plot of $[-\ln(1-\alpha)]$ vs. t, where α is the fractional decomposition of γ-AlH_3. (c) ^{27}Al MAS NMR spectra showing the 2nd and 3rd spinning sidebands at t = 1 h and 192 h, those of the α-AlH_3, and spectrum after subtraction of the α-AlH_3 from the spectrum at t = 192 h. (d) ^{27}Al MAS NMR spectra obtained for decomposition of the γ-AlH_3 phase at high temperatures.

present work, we focus on showing a decomposition reaction of the γ-AlH_3 phase at room temperature. The most important issue in this study is to elucidate the decomposition pathway in addition to obtaining the rate, i.e., to determine possible phase transition from the γ phase to the α phase at room temperature, and possible direct decomposition of the γ phase.

Fig. 2(a) shows a series of ^{27}Al NMR spectra recorded at room temperature over the decomposition time period for the centerband (−20 to 50 ppm) and for Al(M) at 1640 ppm. From the integrated area of the γ-AlH_3 (γ-I and γ-II sites, *vide supra*) and forming Al(M) and α-AlH_3, mole fraction (ϕ) of each species was calculated and plotted as a function of time in Fig. 2(b). The decomposition kinetics of the γ-AlH_3 was analyzed by using the Avrami–Erofeev equation considering the reaction as an irreversible isothermal decomposition, as employed by Graetz et al. [1,2] who recently reported high temperature decomposition of α, β, γ-AlH_3 phases. A plot of $\ln[-\ln(1-\alpha)]$ versus $\ln(t)$, with α being the fractional decomposition, in the current study yielded a value of $n \sim 1$, and $[-\ln(1-\alpha)]$ versus t produced an acceptable liner plot as shown in Fig. 2(b). The result indicates that the rate determining step might be considered in the nucleation and growth model [26], and the growth dimension in this case could be one dimension unlike the previous cases found at high temperatures [1,2]. It is quite interesting because this finding could support that the gamma phase, which has a clear one-dimensional morphology in SEM images [27], actually decompose and nucleate Al in one dimension at low temperatures. The rate constant k obtained from $[-\ln(1-\alpha)]$ versus t plot was $5.8\ (\pm 0.2) \times 10^{-7}\ s^{-1}$, which is an order of magnitude smaller than that at 60 °C [1,2]. The γ-AlH_3 material (BNL-3013) used in this study was found to contain a similar level of contaminants to our previous γ-AlH_3 material (H2990, see above), including α-AlH_3 (∼7%). Recording of ^{27}Al NMR spectra was terminated when hydrogen pressure build-up led opening of the tight-sealing kel-F cap from the rotor.

In order to observe a phase change to the α-AlH_3 phase from the starting γ-AlH_3 phase during room temperature decomposition, spinning sidebands were carefully examined because the centerband of ^{27}Al resonance cannot distinguish α-AlH_3 from the γ-I site as shown in Fig. 2(a). The 2nd and 3rd spinning sidebands (200–400 ppm) of two spectra in Fig. 2(a) are separately displayed in Fig. 2(c) to show the growth of peaks marked by arrows after 192 h at room temperature. Their positions are precisely matched with sideband positions of the α-AlH_3 spectrum shown in Fig. 2(c) (broken line). This result clearly indicates that the phase changes from the γ-AlH_3 to the α-AlH_3 takes places even at room temperature. The bottom spectrum of Fig. 2(c) was generated by subtracting the α-AlH_3 component from the spectrum of 192 h. The subtracted spectrum shows almost identical lineshapes to the top spectrum of 1 h as anticipated with an exception of the reduced intensity. Such phase transition can be easily visualized by NMR at high temperatures as shown in Fig. 2(d), where spinning sidebands manifold of the γ-AlH_3 is greatly reduced to form sidebands manifold of the α-AlH_3 phase at 373 K. Considering the stable nature of the α phase, results presented in Fig. 2 strongly support the view that direct decomposition of the γ-AlH_3 phase to form Al metal also takes place at room temperature. Finally, note that detail analyses of spectra in Fig. 2(a) revealed that the decomposition of the γ-AlH_3 led the formation of both α-AlH_3 and Al metal at about equal amount as plotted in Fig. 2(b).

5. Conclusions

Static and MAS NMR characterization was performed on various AlH_3 samples. ^{27}Al MAS NMR demonstrated high sensitivity in distinguishing local environments of aluminum nucleus depending on the type of connectivity of AlH_6 octahedra and their spatial arrangement. For example, NMR responded with well-resolved lines for corner-sharing and edge sharing AlH_6 octahedra in the γ-AlH_3 polymorph. Once characterized, NMR spectra were useful in the study of the decomposition kinetics and phase transitions taking place in these materials. The reaction rate at room temperature was obtained for unstable γ phase undergoing decomposition. The rate-limiting mechanism appears to be the nucleation and growth model with the dimensionality of one at room temperature. A phase transition to the α phase was also confirmed by analyzing spinning sideband patterns. NMR evidence for direct decomposition of the γ phase at room temperature was also obtained.

Acknowledgements

This research was partially performed at the Jet Propulsion Laboratory, which is operated by the California Institute of Technology under contract with the NASA. This work was partially supported by DOE through Award Number DE-AI-01-05EE11105. The NMR facility at Caltech was supported by the National Science Foundation (NSF) under Grant Number 9724240 and partially supported by the MRSEC Program of the NSF under Award Number DMR-0080065. This work was supported at BNL by the DOE under contract DEA-AC0298CH100886. Financial support received from the Office of Hydrogen, Fuel Cells and Infrastructure Technologies of US Department of Energy is gratefully acknowledged. We thank J.G. Kulleck (JPL) for his X-ray diffraction measurements and Dr. X. Tang from the United Technologies Research Center for providing the Russian made α-AlH_3 material labeled UTRC. Finally, the authors are very grateful to Drs. H. Brinks and V.A. Yartys for providing their detailed crystal structure results to us prior to publication.

References

[1] J. Graetz, J.J. Reilly, J. Phys. Chem. B 109 (2005) 22181.
[2] J. Graetz, J. Reilly, G. Sandrock, J. Johnson, W.M. Zhou, J. Wegrzyn, in: D. Chandra, J.J. Petrovic, R. Bautista, A. Imam (Eds.), Advanced Materials for Energy Conversion III, The Minerals, Metals, and Materials Society, Warrendale, PA, 2006, pp. 57–63.
[3] J.P. Maehlen, V.A. Yartys, in: D. Chandra, J.J. Petrovic, R. Bautista, A. Imam (Eds.), Advanced Materials for Energy Conversion III, The Minerals, Metals, and Materials Society, Warrendale, PA, 2006, pp. 77–85.
[4] V.P. Tarasov, Y.B. Muravlev, S.I. Bakum, A.V. Novikov, Doklady Phys. Chem. 393 (2003) 353–356.
[5] J. Graetz, J.J. Reilly, J. Alloys Compd. 424 (2006) 262.

[6] G. Sandrock, J. Reilly, J. Graetz, W. Zhou, J. Johnson, J. Wegrzyn, Appl. Phys. A 80 (2005) 687.
[7] G. Sandrock, J. Reilly, J. Graetz, W. Zhou, J. Johnson, J. Wegrzyn, J. Alloys Compd. 142 (2006) 185–189.
[8] S.-J. Hwang, R.C. Bowman, J. Graetz, J.J. Reilly, in: J.C.F. Wang, W. Tumas, A. Rougier, M.J. Heben, E. Akiba (Eds.), Hydrogen Storage Materials, Mater. Res. Soc. Symp. Proc., vol. 927E, Warrendale, PA, 2006, pp. 0927-EE03-03.
[9] H.W. Brinks, W. Langley, C.M. Jensen, J. Graetz, J.J. Reily, B.C. Hauback, J. Alloys Compd. 433 (2007) 180.
[10] H.W. Brinks, W. Langley, C.M. Jensen, J. Graetz, J.J. Reily, B.C. Hauback, unpublished.
[11] H.W. Brinks, A. Istad-Lem, B.C. Hauback, J. Phys. Chem. 110 (2006) 25833.
[12] V.A. Yartys, R.V. Denys, J.P. Maehlen, C.h. Frommen, M. Fichtner, B.M. Bulychev, H. Emerich, Inorg. Chem. 46 (2007) 1051.
[13] F.M. Brower, N.E. Matzek, P.F. Reigler, H.W. Rinn, C.B. Roberts, D.L. Schmidt, J.A. Snover, K. Terada, J. Am. Chem. Soc. 98 (1976) 2450.
[14] J.W. Turley, H.W. Rinn, Inorg. Chem. 8 (1968) 18.
[15] O.J. Zogal, B. Stalinski, S. Idziak, Z. Physk. Chem. N.F. 145 (1985) 167.
[16] O.J. Zogal, M. Punkkinen, E.E. Ylinen, B. Stalinski, J. Phys.: Condens. Matter 2 (1990) (1941).
[17] J.W. Wiench, V.P. Balema, V.K. Pecharsky, M. Pruski, J. Solid State Chem. 177 (2004) 648.
[18] B. Bogdanović, M. Felderhoff, M. Germann, M. Härtel, A. Pommerin, F. Schuth, C. Weidenthaler, B. Zibrowius, J. Alloys Compd. 350 (2003) 246.
[19] J.L. Herberg, R.S. Maxwell, E.H. Majzoub, J. Alloys Compd. 417 (2006) 39.
[20] L. Frydman, J.S. Harwood, J. Am. Chem. Soc. 117 (1995) 5367.
[21] J.P. Amoureus, M. Pruski, in: D.M. Grant, R.K. Harris (Eds.), Encyclopedia of NMR, 9, John Wiley & Sons, Chichester, 2002, pp. 226–251.
[22] For all the α-AlH_3 phase studied in the present work, the formation of surface oxide layer was too slow to be detected by NMR.
[23] A.E. Bennett, C.M. Rienstra, M. Auger, K.V. Lakshmi, R.G. Griffin, J. Chem. Phys. 103 (1995) 6951.
[24] J.P. Amoureux, C. Fernandez, Solid State NMR 10 (1998) 211.
[25] J.P. Amoureux, C. Fernandez, L. Carpentier, E. Cochon, Phys. Stat. Sol. (a) 132 (1992) 461.
[26] C.H. Bamford, C.F.H. Tipper (Eds.), Comprehensive Chemical Kinetics, vol. 22, Elsevier, New York, 1980 (Chapter 3).
[27] G.K. Lund, M.W. Lesley, S.R. Glaitli, Proceedings of the JANNF-32nd PEDCS Meeting, 2004, p. 1.